Taylor & Francis
Taylor & Francis Group

RESEARCH ARTICLE

OPEN ACCESS · Check for updates

PLGA microsphere-based composite hydrogel for dual delivery of ciprofloxacin and ginsenoside Rh2 to treat *Staphylococcus aureus*-induced skin infections

Minghao Sun[a*], Chune Zhu[b*], Jieyu Long[a], Chao Lu[a,c] (iD), Xin Pan[a] (iD) and Chuanbin Wu[a,c] (iD)

[a]School of Pharmaceutical Sciences, Sun Yat-sen University, Guangzhou, China; [b]School of Traditional Chinese Medicine, Guangdong Pharmaceutical University, Guangzhou, China; [c]College of Pharmacy, Jinan University, Guangzhou, China

ABSTRACT

When antibiotic-resistant pathogenic bacteria pose a high threat to human health, bacterial multidrug efflux pumps become major contributors to the high-level antibiotic resistance in most microorganisms. Since traditional antibiotics are still indispensable currently, we report a dual drug delivery system to maximize the antibacterial efficacy of antibiotics by inhibiting efflux pumps in bacteria before their exposure to antibiotics. In this research, a microsphere/hydrogel composite was constructed from ciprofloxacin (Cip)-loaded poly (lactic-*co*-glycolic acid) (PLGA) microspheres and ginsenoside Rh2 (G-Rh2) dispersed thermo-sensitive hydrogel to treat skin infections. *In vitro* drug release studies indicated that while G-Rh2 in hydrogel presented a faster and short-term release manner to rapidly inhibit the NorA efflux pumps, Cip showed a sustained and long-term release behavior to provide a local high concentration gradient for facilitating drug percutaneous penetration. The combination of Cip and G-Rh2 demonstrated a high degree of synergism against both methicillin-sensitive *Staphylococcus aureus* (MSSA) and methicillin-resistant *Staphylococcus aureus* (MRSA), hence significantly improving their *in vitro* antibacterial activity and efficiency. Moreover, the antibacterial performance of the microsphere/hydrogel composite with a sequential release profile is superior to that of other formulations in mouse model of MRSA skin infections, indicating its great potential to treat antibiotic-resistant skin infections.

1. Introduction

Staphylococcus aureus (*S. aureus*) is one of the main pathogens and involved in a vast majority of infections (Tong et al., 2015; Rowe et al., 2020). With the development of antibiotic resistance, methicillin-resistant *S. aureus* (MRSA) has become one of the most frequent causes of hospital- and community-associated infections (Lakhundi & Zhang, 2018). The U.S. Centers for Disease Control and Prevention (CDC) estimates that antibiotic-resistant bacteria cause at least 2 million illnesses and approximately 23 thousand deaths every year in the United States (Pei et al., 2017; Lu et al., 2019). Gram-positive pathogens are responsible for the majority of cases of acute bacterial skin and skin structure infections, and a significant proportion of which in the United States are MRSA (Russo et al., 2016; Mir et al., 2019). Therefore, it is urgent to find a strategy to cope with the health threats posed by MRSA-induced skin infections (Li et al., 2015).

Though literature has reported many novel antibacterial agents (Li et al., 2015; Mei et al., 2017; Gold et al., 2018), traditional antibiotics are still indispensable in a short term due to the high costs, long cycles and big risks in novel antibiotics development (Årdal et al., 2019). Therefore, the combination of antibiotics and other drugs may be a more reasonable alternative strategy to enhance the susceptibility of bacteria, reduce the occurrence of drug resistance, and even reverse bacterial resistance to antibiotics (Wright, 2017). Recently, Langeveld et al. (Langeveld et al., 2014) indicated that some essential oils and their components had synergistic effect in combination with antibiotics, which may offer possibilities for reducing dosage. Sathiya et al. (Deepika et al., 2018) demonstrated that rutin, a natural compound isolated from *Ruta graveolens*, displayed enhanced anti-biofilm property when combined with conventional antibiotic gentamicin. Singh et al. (Singh et al., 2017) found that boeravinone B could act as NorA efflux pump inhibitors to effectively retain higher concentrations of ciprofloxacin (Cip) in *S. aureus*.

Multidrug resistant efflux pumps are recognized as important components of resistance in both Gram-positive and Gram-negative bacteria, which reduce the intracellular concentration of drug compounds through active extrusion from the cell (Fernández & Hancock, 2012; Du et al., 2018). In *S. aureus*, several multidrug efflux pumps, such as NorA, NorB and MepA, have been described that are associated with resistance to antibiotics, and NorA is the most

important and well characterized efflux pump (Holler et al. 2012; Astolfi et al., 2017; Felicetti et al., 2017; Felicetti et al., 2018). It is reported that the stable hydrogen bonding interactions between ginsenoside Rh2 (G-Rh2) and Gln51/Asn340/Ser226 residues at active binding site in the central cavity of protein was responsible for the inhibition of NorA pump, thus G-Rh2 could be used as an inhibitor of the NorA efflux pump to restore susceptibility to common antibiotics in multiple drug resistant (MDR) bacteria (Zhang et al., 2014; Shriram et al., 2018; Kumar et al., 2020). Meanwhile, G-Rh2 is one of the active compounds extracted from ginseng, exhibiting unique immune enhancement effect different from other efflux pump inhibitors (Lee et al., 2018). It is reported that exposure to a given antibiotic can induce the bacterium cell to synthesize more efflux pump units, thus adding additional survival advantage to the cell (Schindler et al., 2015; Foster, 2017; Willers et al., 2017). Therefore, inhibiting the efflux pumps in bacteria before their exposure to antibiotics may be a reasonable strategy to maximize the antibacterial effect, which inhibits antibiotic ejection in early stage, further increases intracellular concentrations of antibiotics, and enhances susceptibility of bacteria.

In this work, we present a poly (lactic-co-glycolic acid) (PLGA) microsphere-based composite thermo-sensitive hydrogel system for dual delivery of Cip and G-Rh2 as a dual drug release vehicle (Cip-MS-G-TSG). Cip was chosen as a model drug to be encapsulated in PLGA microspheres, as the NorA efflux pumps are considered as contributors to Cip resistance (Redgrave et al., 2014; Palazzotti et al., 2019). Thermo-sensitive hydrogel (TSG), a liquid formulation which could be transformed to hydrogel by body temperature heating, was used to encapsulate the bacterial NorA efflux pump inhibitor G-Rh2. It is expected that the obtained Cip-MS-G-TSG presented a sequential release profile. While G-Rh2 in TSG presented a faster and short-term release manner to rapidly inhibit the NorA efflux pumps, Cip showed a sustained and long-term release behavior to provide a local high concentration gradient for facilitating drug percutaneous penetration. The combinational effect of Cip and G-Rh2 was evidenced on methicillin-sensitive *S. aureus* (MSSA) and MRSA strains. The antibacterial efficacy of Cip-MS-G-TSG was further investigated by *in vitro* bacterial killing kinetics assay and *in vivo* mice skin infection models.

2. Materials and methods

2.1. Materials

Ciprofloxacin hydrochloride hydrate (98% purity) and poly (vinyl alcohol) (PVA, 1788 type) were purchased from Aladdin (Shanghai, China). Ciprofloxacin Hydrochloride Gel (CHG) was purchased from Beijing Twinluck Pharmaceutical Co., Ltd. (Beijing, China). PLGA (lactic: glycolic acid = 50: 50, Mw 6.4 kDa) was purchased from Daigang Biology (Jinan, China). Ginsenoside 20(S)-Rh2 was obtained from Meilun Biotechnology (Dalian, China). Poloxamer 407 and poloxamer 188 were offered by Aike, Reagent (Zhejiang, China).

Hyaluronic acid (HA, Mw 3.5 kDa) was purchased from Bloomage Biotechnology (Jinan, China). MSSA (ATCC 25923) and MRSA (ATCC 33591) were obtained from ATCC (USA).

2.2. Preparation and characterization of PLGA microspheres

A water-in-oil-in-water (w/o/w) double emulsion/evaporation technique was used for Cip-loaded PLGA microspheres (Cip-MS) fabrication (Zhu et al., 2015). Briefly, 20 mg of Cip were dissolved in 0.5 mL of deionized water and emulsified with 5 mL of a 80 mg/mL PLGA ethyl acetate solution under sonication with an ice bath for 2 min. Subsequently, the resulting primary emulsion (w/o) was mixed with 50 mL of a 5% (w/v) PVA aqueous solution and homogenized at 10,000 rpm using an emulsifier (FA25, Fluko, Germany) with an ice bath for 30 s. The obtained secondary emulsion (w/o/w) was poured into 500 mL of 10% (w/v) NaCl aqueous solution and stirred at 400 rpm overnight at room temperature to evaporate the organic solvent and harden the microspheres. The resulting Cip-MS were collected by centrifugation at 4,000 rpm for 5 min and washed three times with deionized water. Cip-MS were lyophilized to harvest dry powder microspheres for further evaluation.

The surface morphology of Cip-MS was examined by a scanning electron microscope (SEM, JSM 6330 F, JEOL Ltd., Japan) at an accelerating voltage of $10 \sim 20$ kV. Dried microsphere samples were mounted on a copper grid and sputter-coated with gold in a high vacuum evaporator prior to observation.

Particle size and polydispersity of Cip-MS were measured by a Laser Diffraction Malvern Master Sizer 2000 (Malvern Instruments, Britain). The polydispersity was presented as S_{pan} factor calculated from the Equation (1):

$$S_{pan} = (d_{90} - d_{10})/d_{50} \tag{1}$$

Where d_{10}, d_{50}, and d_{90} are microparticle diameters below which 10, 50, and 90% of the volume of microspheres lie, respectively.

For zeta potential determination, Cip-MS were suspended in deionized water, diluted to count rate of 200–300 and characterized by a Zetasizer (ZS90, Malvern Instruments, Britain) before test. Samples were measured in triplicate.

To evaluate the loading efficiency (LE) and encapsulating efficiency (EE) of Cip-MS, approximately 10 mg of samples of three triplicate were accurately weighed and dissolved in 2 mL of dimethyl sulfoxide. The obtained solution was subsequently filtered and subjected to HPLC determination (Ultra Violet detector, Shimadzu, Japan) with a C18 reversed-phase column (Kinetex®, Phenomenex, America). The mobile phase for Cip was a mixture of phosphoric acid (pH = 3.0 ± 0.1) -acetonitrile (87:13, v/v) pumped at a rate of 1.5 mL/min. Detection was performed at the wavelength of 278 nm. The chromatograph was analyzed by Thermo Scientific™ Dionex™ Chromeleon™ Chromatography Data System (Vanquish UHPLC, ThermoFisher, America). LE and EE of

Cip-MS were calculated from the Equation (2) and (3):

$$\text{Loading efficiency (LE\%)} = \frac{\text{Weight of Cip in Cip}-\text{MS}}{\text{Weight of Cip}-\text{MS}}$$
$$\times 100\% \qquad (2)$$

$$\text{Encapsulating efficiency (EE\%)}$$
$$= \frac{\text{Weight of Cip in Cip}-\text{MS}}{\text{Weight of Cip initially added}} \times 100\% \qquad (3)$$

2.3. Preparation and characterization of TSG and Cip-MS-G-TSG

The matrix of TSG consisted of poloxamer and HA. The concentrations have been adjusted according to gelation and rheological characteristics of obtained TSG. Briefly, 20.32% (w/v) poloxamer 407 and 0.98% (w/v) poloxamer 188 were dissolved into deionized water and the mixture was stirred at 400 rpm till complete dissolution. HA (4.88%, w/v) was subsequently added to the mixture. Afterwards, TSG was cooled at 4 °C for 30 min and filtered to clarification. At temperature below the gelation point, Cip-MS were suspended into TSG, while G-Rh2 was directly dissolved in the mixture to obtain the Cip-MS-G-TSG pre-gel solution.

The pH value of TSG pre-gel solution was measured by a pH meter (PB-10, Sartorius, Germany) at room temperature. The gelation temperature was measured by a tube inversion method as described by Zeng et al. (2018). Briefly, a tube with TSG pre-gel solution inside was heated in water bath at a rate of 1 °C/min. The tube was inverted at fixed time points to observe the fluidity of the formulation. The gelation temperature was taken to be the temperature at which there was no flow upon inversion of the tube (Matthew et al., 2002). For gelation time measurement, the tube with an iron wire and TSG pre-gel solution inside was kept in water bath at gelation temperature under magnetic stirring at 50 rpm. Once the iron wire stopped stirring, the corresponding time interval was recorded as the gelation time. Each measurement mentioned above was replicated thrice.

2.4. Rheological test of TSG

All rheological tests of TSG were studied using a Rheometer (Kinexus, Malvern Instruments, Britain). The variation of shear viscosity with shear rate was determined. Briefly, 1 mL of TSG samples were equilibrated at room temperature (20 °C) and body surface temperature (33 °C), respectively. The shear rate was programed to increase from $0.1\,s^{-1}$ to $100\,s^{-1}$ at a rate of $50\,s^{-1}$/min to obtain the viscosity curve. The viscosity properties of CHG were measured by the same program to be set as a control.

Thixotropy test was employed at 33 °C. TSG was initially equilibrated at a shear rate of $0.1\,s^{-1}$. Subsequently, a programed strength at a shear rate of $100\,s^{-1}$ was applied for 30 s and withdrew immediately as an estimate of viscosity recovery in contrast with CHG.

Viscoelasticity were presented as the elastic modulus (G′) and viscous modulus (G″). The temperature was programed to increase from 25 °C to 40 °C at a rate of 1 °C/min to determine the critical temperature at which G′ equaled G″.

2.5. In vitro cumulative release

In vitro release studies of various formulations were carried out using a dialysis method. Briefly, approximately 1 g of each formulation ($n = 3$) was enclosed in a dialysis bag (Mw cut off 2 kDa, Solarbio, China). The dialysis bag was immersed in 10 mL of PBS (pH = 7.4, containing 0.2% Tween 80) and incubated at 37 °C under gentle shaking at 100 rpm. At predetermined time points, all the release media was removed and replenished by fresh PBS. The aliquots were filtered and the concentration of Cip and G-Rh2 was determined by HPLC analysis. As a contrast, a co-delivery system of TSG encapsulating Cip and G-Rh2 (Cip-G-TSG) was prepared and the *in vitro* release behavior was performed by the same method.

2.6. In vitro cytotoxicity studies

The cytotoxicity of Cip-MS-G-TSG was employed on HaCaT cell lines, obtained from Chinese Academy of Sciences. Cells were cultivated in Dulbecco's Modified Eagle Medium (DMEM) supplemented with 10% fetal bovine serum (FBS), 100 units/mL penicillin and 100 μg/mL streptomycin at 37 °C in humidified incubator (HERAcell, ThermoFisher, America) with 95% air and 5% CO_2. Cells were seeded in a 96-well plate at a density of 5×10^3 per well and incubated for 24 h. Afterwards, the growth medium was incubated with different concentrations of Cip-MS-G-TSG or PBS solution in DMEM containing 10% FBS. After 24 and 48 h incubation, the cell viability was characterized by Thiazolyl Blue Tetrazolium Bromide (MTT) colorimetric assays. The optical absorbance of each well ($n = 6$) was measured at 490 nm using a Microplate Absorbance Reader (ELX800, BioTek Instruments, America).

2.7. Minimum inhibitory concentration (MIC) and minimum bactericidal concentration (MBC)

Broth microdilution test was performed to determine the MIC of Cip, G-Rh2 and the combination of Cip and G-Rh2, respectively. MSSA or MRSA strains were regenerated in 10 mL Mueller-Hinton Broth (MHB, CM0337, Oxoid, Britain) medium at 37 °C with gentle shaking (Humidified Incubator, BSD-250, Boxun, China, supplemented with 95% air and 5% CO_2) for 12 h. Strains suspension was diluted to 2×10^5 colony forming units per mL (CFU/mL) and seeded in a 96-well plate at total volume of 50 μL per well. Cip, G-Rh2 or the mixture of Cip and G-Rh2 were added at the same volume by serially dilution. Following 8 h incubation, the optical density (OD) of each well was measured at 630 nm. The lowest drug concentration to produce an OD < 0.1 was considered as the MIC. Lastly, the content of wells which produced OD < 0.1 was resuspended. 10 μL suspension of each well was removed into Mueller-Hinton Agar (MHA, CM0405,

Oxoid, Britain) media for 18 h incubation to observe the bacterial growth. The lowest concentration at which no bacterial growth occurred was considered as the MBC.

2.8. Killing kinetics assays

MSSA or MRSA strains were regenerated, diluted to 2×10^6 CFU/mL in a conical flask and then treated with PBS, TSG encapsulating blank MS (MS-TSG), Cip and G-Rh2 mixed solution (Cip-G-Solution), Cip-G-TSG and Cip-MS-G-TSG, respectively. The concentration of Cip and G-Rh2 were $10 \times$ MIC for the latter three groups. At predetermined intervals, 10 μL suspension of each group ($n = 3$) was removed, serially diluted and embedded in MHA media in triplicate. Following 12 h incubation, the viable colonies on the plates were counted to calculate the concentration of viable bacteria.

2.9. In vivo *antibacterial assessment*

A mouse model of MRSA skin infection was used to determine the *in vivo* antibacterial activity of Cip-MS-G-TSG. Balb/c male mice (5–8 weeks, weighing 20–30 g) of SPF grade were obtained from Lavatory Animal Center, Sun Yat-sen University. Commercial regular diet and water were supplied *ad libitum*. The research protocol was approved by the Institutional Animal Care and Use Committee, Sun Yat-sen University, with Approval No. SYSU-IACUC-2019-000321.

One day preceding the study, mice were randomly divided into 6 groups and anesthetized by 1% (w/v) sodium pentobarbital (50 mg/kg). The back hairs were shaved by depilatory cream. Afterwards, the epidermis was tape-stripped to rubedo and errhysis. 1×10^7 CFU/mL of MRSA suspension was applied to the skin. Each group was *in situ* treated with 1 mL PBS, blank MS-TSG, CHG, Cip-G-Solution, Cip-G-TSG and Cip-MS-G-TSG for 5 days, respectively. The concentration of Cip and G-Rh2 were $50 \times$ MIC for the latter three groups. At predetermined time points, mice of each group ($n = 6$) were sacrificed by euthanasia, and their tissues of infected areas were removed, homogenized, serially diluted and embedded in MHA plates for 12 h. The viable colonies were counted to calculate the concentration of residual viable bacteria.

To evaluate the inflammatory reaction in mice skin, on day 5, the skin homogenates from 4 typical groups (PBS, Cip-G-Solution, Cip-G-TSG and Cip-MS-G-TSG) were centrifuged at 12,000 rpm for 10 min. The supernatant was collected and mixed with chloroform. The mixture was further centrifuged and the precipitation was resuspended with isopropanol. Then, the suspension was centrifuged at 12,000 rpm for 5 min to harvest mRNA precipitation. Extracted mRNA was washed by 75% ethanol, dried, dissolved in deionized water and incubated at 55 °C before test. Total RNA was reverse transcribed by a fluorescent quantitation PCR machine (Stepone plus, ABI, America) and amplification was conducted under the following circulation: 95 °C to 60 °C in 15 s, 60 °C for 60 s, repeated for 40 times. Mice without MRSA infection treatment were set as the control group (Blank) and glyceraldehyde-3-phosphate dehydrogenase (GAPDH) was selected as the reference gene to normalize the mRNA level of tumor necrosis factor (TNF-α), interleukin 6 (IL-6) and interleukin 1 beta (IL-1β), respectively.

For histology evaluation, skin tissue specimens of infected areas from the above mentioned 4 typical groups were harvested and fixed in 4% (w/v) paraformaldehyde. Tissue samples were embedded in paraffin, sectioned and stained with hematoxylin and eosin (H&E) for histology. Sections were examined and captured with a Microscope (Eclipse Cl, Nikon, Japan).

2.10. Statistical analysis

Data were was expressed as mean ± standard deviation (Mean ± S.D). Statistical differences between the experimental and control groups were evaluated with a paired *t*-test and $p < .05$ was considered statistical different.

3. Results and discussion

3.1. Characterization of Cip-MS

Among pharmaceutical polymers, biodegradable PLGA has gained great attention in design of various drug loaded devices (Mona et al., 2020). PLGA microspheres for the sustained release of Cip were thus prepared by the double emulsion/evaporation method. As shown in Figure 1(A,B), Cip-MS had spherical shapes with smooth surfaces. No breakage, wrinkle or aggregation was observed, indicating the high stability of microspheres during fabrication and lyophillization. According to particle size analysis data, the mean particle size (d_{50}) of Cip-MS was 1.86 ± 0.29 μm, and the relatively low S_{pan} value (2.51 ± 0.84) suggested a quite narrow size distribution. Besides, Cip-MS exhibited neutral zeta potential (0.81 ± 0.39 mV). The LE and EE of Cip-MS were $3.17 \pm 0.19\%$ and $69.76 \pm 4.11\%$, respectively.

3.2. Characterization of TSG and Cip-MS-G-TSG

TSG has been developed for drug encapsulation and surgical dressing due to its unique performance. Its phase-transition character can support quantified dosage administration, averts superinfection and wound contact, especially for wound and infection treatment (Gao et al., 2019; Xu et al., 2019). Herein, TSG with the main matrix of poloxamer was
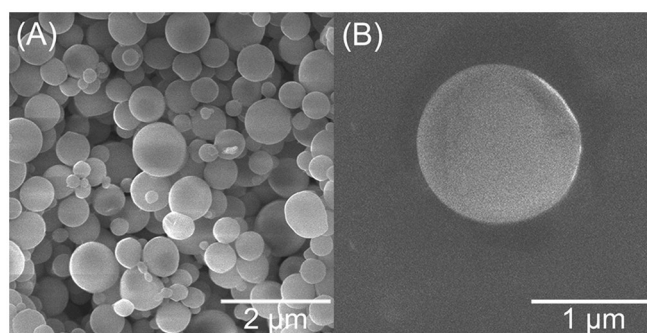
Figure 1. SEM images of Cip-MS in 8,000× (A) and 18000× (B).

prepared. HA was applied to promote moisture retaining, wound healing and tissue regeneration (Sharma et al., 2018). The neutral pH value (7.28 ± 0.18) of TSG pre-gel solution implied its low irritation to human skin. Furthermore, the appearance of TSG and Cip-MS-G-TSG were presented in Figure 2(A–D). We found that TSG was translucent and possessed good mobility at 20 °C, and Cip-MS could be uniformly dispersed in the TSG before and after gelation . In the present study, the gelation temperature of TSG was determined as 32.67 ± 0.29 °C, which was close to the body surface temperature of human being (Liu et al., 2013). The gelation process could be finished within 65.05 ± 3.47 s. Thus, the promptly transition of TSG from solution to gel is convenient for patients to use.

3.3. Rheological properties

The rheological properties in this study generally demonstrate the fluidity change associated with temperature or external force. Herein, the variation of shear viscosity, thixotropy and viscoelasticity were measured, while CHG was set as a control. In Figure 3(A,B), shear viscosity was plotted as a function of shear rate at 20 °C and 33 °C, respectively. Both TSG and CHG exhibited lower shear viscosity at 20 °C, especially for TSG, which could maintain good liquidity below gelation temperature. At 33 °C when TSG was gelled, its shear viscosity remarkably increased and was almost equivalent to that of CHG (Figure 3(B)), in accordance with the phase-transition property.
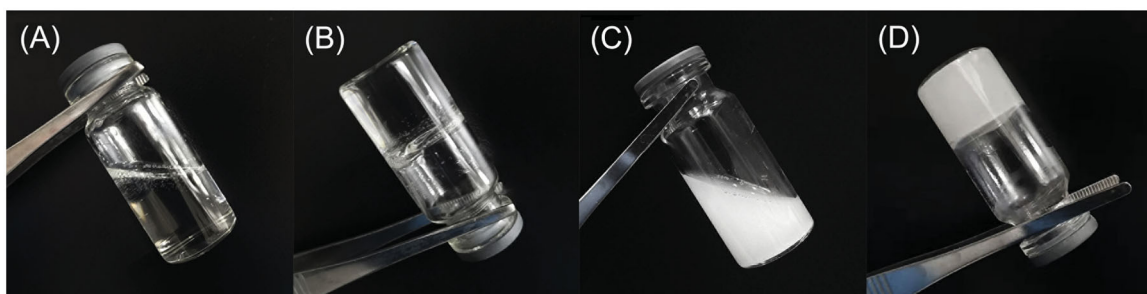
Figure 2. Photos of TSG at 20 °C (A) and 33 °C (B), and photos of Cip-MS-G-TSG at 20 °C (C) and 33 °C (D).
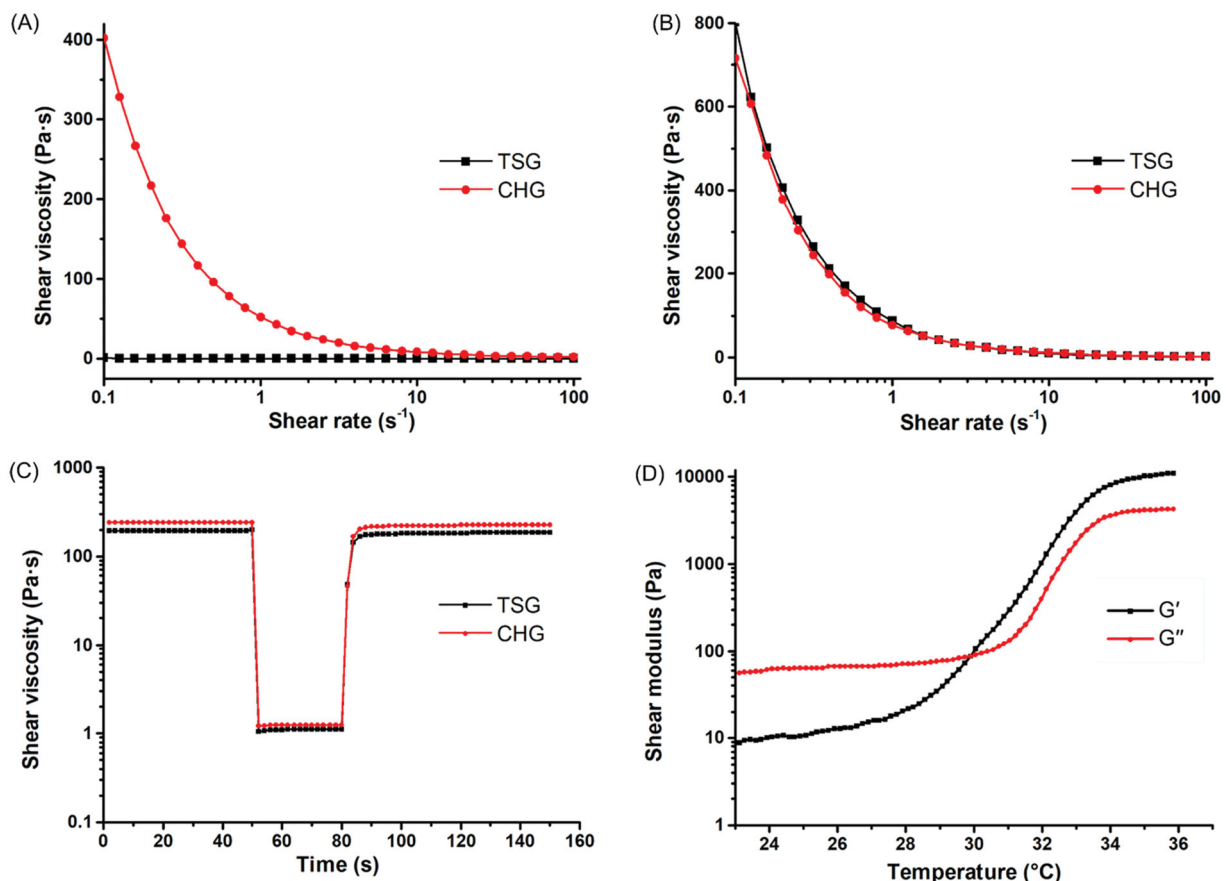
Figure 3. Rheological properties of TSG. (A) Variation of shear viscosity of TSG and CHG at 20 °C. (B) Variation of shear viscosity of TSG and CHG at 33 °C. (C) Thixotropy profile of TSG and CHG. (D) Variation of G′ and G″ of TSG with temperature.

Thixotropy test was to illustrate the decrease of viscosity induced by flow and shear viscosity recovery when the flow is discontinued. As shown in Figure 3(C), the shear viscosity of both TSG and CHG decreased to a steady level within 30 s of stress application. However, the viscosity recovered promptly after external force withdrew. The result validated decent viscous restoration and resilient capability of TSG.

G′ and G″ of TSG were plotted as a function of temperature shown in Figure 3(D). As the temperature increased, the two coefficients went up accordingly. At approximate 29.8 °C, G′ value exceeded G″ value, indicating a elastic solid-like behavior. This critical temperature was lower than the gelation temperature measured by the tube inversion method. Actually, TSG still possessed fluidity at around this temperature until it was completely gelled at 32.67 °C. Taken together, these studies demonstrated that TSG showed advantageous rheological properties for local application.

3.4. In vitro *drug release behaviors*

Figure 4 showed typical release profiles of Cip and G-Rh2 from Cip-MS-G-TSG and Cip-G-TSG dual drug delivery systems. G-Rh2 exhibited a short-term release behavior, while Cip from the Cip-MS-G-TSG presented a sustained and long-term release behavior. Comparing with the G-Rh2 release profiles in Figure 4(A,B), we found that the release patterns of G-Rh2 were very similar. G-Rh2 could be completely released from the hydrogel matrix within 48 h, indicating that the introduction of Cip-MS or Cip exhibited negligible impact on G-Rh2 release. The rapid release profile of Cip in Cip-G-TSG was similar to that of G-Rh2, whereas Cip showed sustained release from Cip-MS-G-TSG for 12 days, suggesting that the sustained long-term release behavior of Cip was mainly controlled by the PLGA microspheres. Consequently, a sequential-release behavior was achieved in the PLGA microsphere-based composite hydrogel system. It is expected that G-Rh2 could rapidly inhibit bacterial efflux pump, while Cip could be released in a sustained manner to provide a local high concentration gradient for facilitating drug percutaneous penetration.

3.5. Cytotoxicity test

The cytotoxicity was examined by MTT assay in HaCaT cell lines. Cells were incubated with Cip-MS-G-TSG at concentrations of 0–50 mg/mL, and no obvious cell death was observed within 24 h or 48 h incubation (Figure 5). This result further verified the biocompatibility of Cip-MS-G-TSG.

3.6. In vitro *antibacterial activity studies*

G-Rh2 has been reported to exert antibacterial action and synergize antibiotics (Zhang et al., 2014; Cao et al., 2019; Xue et al., 2020). To evaluate the antibacterial effects of the G-Rh2-antibiotics combination, the MIC and MBC were determined for each of the individual components as well as the combination therapy. As shown in Table 1, when the MIC of Cip alone was ranged from 0.25 to 0.50 μg/mL, the addition of G-Rh2 produced a 1-fold to 4-fold decrease in the MIC of Cip. Moreover, according to the MBC of Cip, which ranged from 1 to 2 μg/mL, the addition of G-Rh2 resulted in a 4-fold to 8-fold decrease in the MBC of Cip. The sum of the fractional bactericidal concentration (ΣFBC) indicated the extent
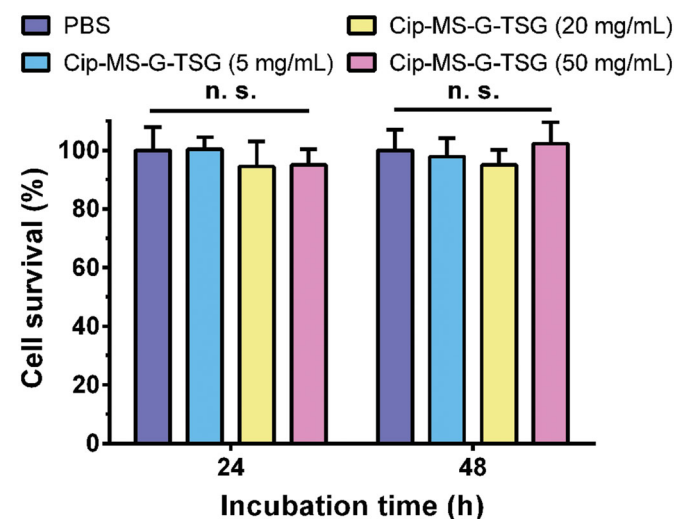
Figure 5. MTT assay of Cip-MS-G-TSG on HaCaT cell lines (mean ± SD, $n = 6$).

Figure 4. *In vitro* cumulative release profiles of Cip-MS-G-TSG (A) and Cip-G-TSG (B) (mean ± SD, $n = 3$), while the insert picture in (A) was the whole release process of Cip from Cip-MS-G-TSG.

Table 1. Antibacterial activity of Cip co-delivered with G-Rh2 against MSSA and MRSA.

	G-Rh2		Cip		Cip + G-Rh2[a]		
Bacteria strains	MIC (µg/mL)	MBC (µg/mL)	MIC (µg/mL)	MBC (µg/mL)	MIC (µg/mL)	MBC (µg/mL)	ΣFBC Index[b] (Effect)[c]
Methicillin-sensitive *S. aureus*	25.00	50.00	0.25	1.00	0.12	0.25	0.38 (S)
Methicillin-resistant *S. aureus*	25.00	50.00	0.50	2.00	0.12	0.25	0.25 (S)

[a]The concentration of G-Rh2 is 6.25 µg/mL;
[b]$\Sigma FBC = MBC_{A,combination}/MBC_{A,alone} + MBC_{B,combination}/MBC_{B,alone}$;
[c]Synergy (S) was defined as ΣFBC index of ≤0.5. Indifference (I) was defined as ΣFBC index of >0.5 but ≤4.0. Antagonism (A) was defined as ΣFBC index of >4.0.
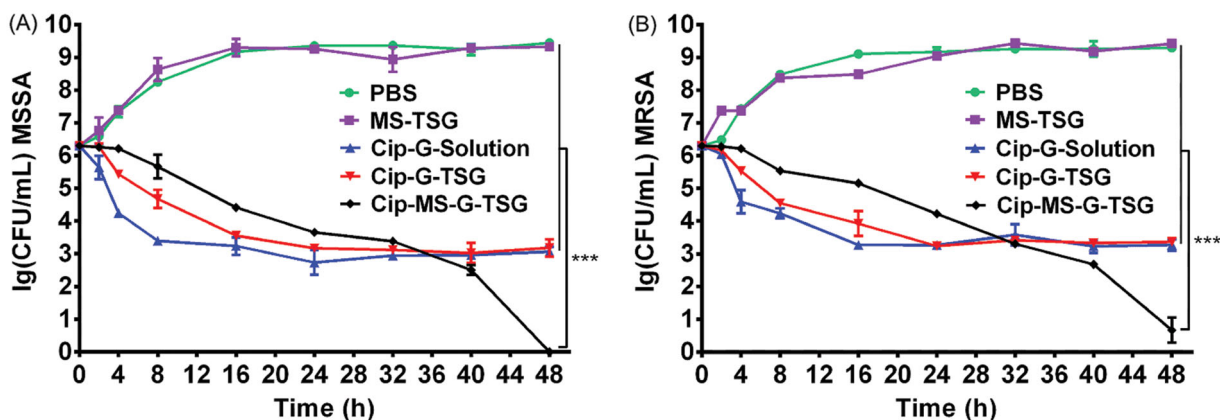
Figure 6. Time-kill curves of various formulations against MSSA (A) and MRSA (B) (mean ± SD, $n = 3$). ***$p < .001$, *vs.* Cip-MS-G-TSG group.

of the interaction between the drugs (Ng et al., 2013), and Cip and G-Rh2 synergy (ΣFBC ≤ 0.5) was found in both MSSA and MRSA. Therefore, G-Rh2 could be applied as an effective adjuvant to synergize Cip.

3.7. In vitro *killing kinetics assays*

To further evaluate the killing efficiency of Cip-MS-G-TSG and illuminate their mechanism of action, a time-kill method was employed. As shown in Figure 6(A,B), MS-TSG had no influence on bacteria growth. Although Cip-G-Solution and Cip-G-TSG without sequential release profile showed fast time-killing rate during the initial 16 h, the concentration of viable bacteria no longer decreased and even appeared slight rising trend after 24 h in these two formulations. Previous studies found that repeated exposure to low concentrations of fluoroquinolone antibiotics such as Cip would lead to activation of the efflux pump systems and a reduction in susceptibility (Cebrián et al., 2005; Redgrave et al., 2014; LaBreck et al., 2020). Therefore, although an initial phase of rapid bacterial killing was induced by the rapid release of Cip from Cip-G-Solution and Cip-G-TSG, both formulations could not kill MSSA or MRSA cells completely in 48 h probably due to their relatively low intra-bacterial accumulation of Cip. Conversely, Cip-MS-G-TSG exhibited enhanced antibacterial efficiency against MSSA and MRSA, eliminating all bacteria completely in 48 h. These results confirmed our hypothesis that administrating efflux pump inhibitor prior to antibiotic application by this microsphere-based composite hydrogel system may be conducive to rapidly control the development of antibiotic resistance before efflux pump activation, and thus maximize the antibacterial effect.

3.8. In vivo *antibacterial efficacy*

A typical mouse skin infection model was established to evaluate the *in vivo* antibacterial efficacy of Cip-MS-G-TSG. Since MRSA has become the most common cause of skin and soft-tissue infections in many parts of the world (Singer & Talan, 2014), it was chosen to cause topical bacterial colonization in this study. As shown in Figure 7(A), when continuous growth of MRSA was observed among PBS and MS-TSG groups within 5 days, commercial gel CHG resulted in significantly reduce in the amount of MRSA remaining in the skin ($p < .01$) at the first day postinfection but could not perform sustained bactericidal effect. Similarly, Cip-G-Solution and Cip-G-TSG no longer performed antibacterial efficiency after day 3. However, Cip-MS-G-TSG killed more than 99.999% of bacteria after 5 days treatment. The amount of MRSA strains remaining in the skin of the Cip-MS-G-TSG-treated mice was 6.46×10^6 times, 1.56×10^3 times, 1.43×10^2 times and 75.5 times lower than those remaining in the MS-TSG-treated mice ($p < .001$), CHG-treated mice ($p < .001$), Cip-G-Solution-treated mice ($p < .001$) and Cip-G-TSG-treated mice ($p < .001$), respectively.

Since inflammation can reflect injury and infection to some degree, TNF-α, IL-6 and IL-1β were selected as indicators to evaluate the inflammatory extent in mice skin. The mRNA expression levels of these inflammatory cytokines in various treatment groups were thus determined on day 5. As shown in Figure 7(B), when MRSA infection dramatically increased the mRNA expression level of all inflammatory cytokines, the skin of Cip-MS-G-TSG-treated mice showed the lowest corresponding level, which further illustrated the optimized therapeutic effect of Cip-MS-G-TSG in the treatment of bacterial infection. Meanwhile, since G-Rh2 has been
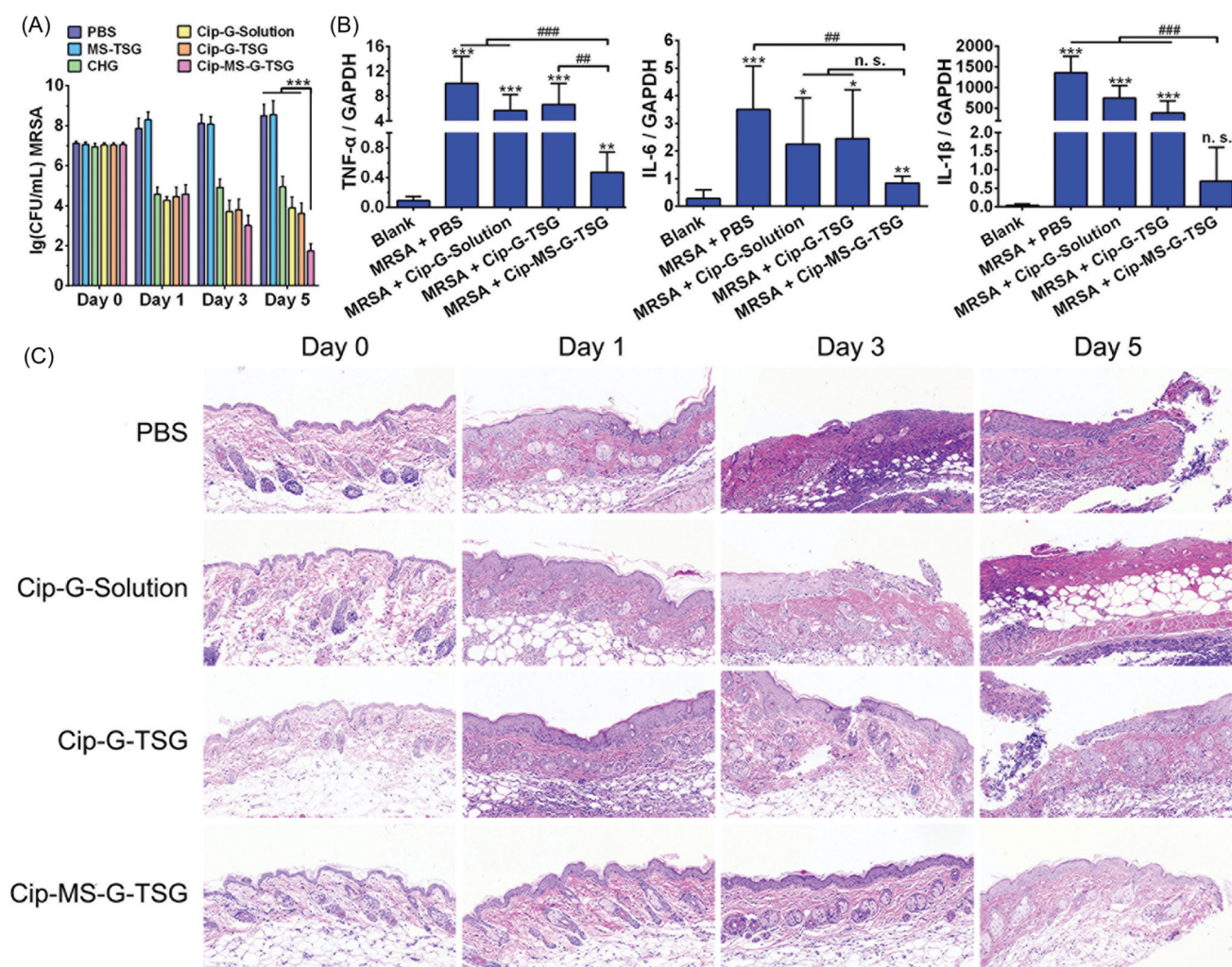
Figure 7. *In vivo* antibacterial study of Cip-MS-G-TSG. (A) Microbial burden in a murine model of skin infection with various treatments (mean ± SD, $n = 6$). ***$p < .001$, *vs.* Cip-MS-G-TSG group. (B) The mRNA expression levels of TNF-α, IL-6 and IL-1β in the uninfected (Blank) and infected skins (mean ± SD, $n = 6$). *$p < .05$, **$p < .01$, ***$p < .001$, *vs.* Blank group. ##$p < .01$, ###$p < .001$, *vs.* Cip-MS-G-TSG group. (C) H&E-stained sections of infected skin with PBS, Cip-G-Solution, Cip-G-TSG and Cip-MS-G-TSG treatments on day 0, 1, 3 and 5, respectively.

reported to possess anti-inflammatory activity (Kim et al., 2017), it may also play an important role in accelerating skin healing.

Furthermore, histological analysis in skin tissue with various treatments were performed by H&E staining (Figure 7(C)). The results indicated that infection-induced damage to the skin of PBS-treated mice increased apparently over time. The skin morphology of Cip-MS-G-TSG-treated mice was nearly identical to the healthy skin on day 5, whereas fester and inflammatory cells infiltration still remained after other treatments. As a whole, all these results illustrated the excellent long-term antibacterial effect of Cip-MS-G-TSG on the *in vivo* treatment of MRSA skin infection in virtue of the sequential release profile.

4. Conclusion

In this research, Cip-MS-G-TSG was prepared as an efficient dual drug delivery system to treat *S. aureus* skin infection. Cip-MS with mean particle size of $1.86 \pm 0.29\,\mu m$ was dispersed into TSG along with G-Rh2. The microsphere-based

composite hydrogel system exhibited optimal rheological properties, low cytotoxicity, and sequential release profile. The synergistic effect of Cip with G-Rh2 against MSSA and MRSA was evidenced. Optimized *in vitro* sterilizing ability was demonstrated by Cip-MS-G-TSG benefited from its sequential release feature. In MRSA skin infection mouse model, Cip-MS-G-TSG achieved outstanding *in vivo* antibacterial efficacy. Above all, these results demonstrated that the novel microsphere/hydrogel composite has excellent potential applications in topical treatment of skin infection.

Disclosure statement

No potential conflict of interest was reported by the author(s).

ORCID

Chao Lu (iD) https://orcid.org/0000-0002-2118-8888
Xin Pan (iD) https://orcid.org/0000-0003-1437-2780
Chuanbin Wu (iD) http://orcid.org/0000-0003-1661-0201

References

Årdal C, Balasegaram M, Laxminarayan R, et al. (2019). Antibiotic development—economic, regulatory and societal challenges. Nat Rev Microbiol.18:267–74.

Astolfi A, Felicetti T, Iraci N, et al. (2017). Pharmacophore-based repositioning of approved drugs as novel *Staphylococcus aureus* NorA efflux pump inhibitors. J Med Chem 60:1598–604.

Cao XX, Ye QL, Fan MW, et al. (2019). Antimicrobial effects of the ginsenoside Rh2 on monospecies and multispecies cariogenic biofilms. J Appl Microbiol 126:740–51.

Cebrián L, Rodríguez JC, Escribano I, et al. (2005). Characterization of *Salmonella spp.* Mutants with reduced fluoroquinolone susceptibility: importance of efflux pump mechanisms. Chemotherapy 51:40–3.

Deepika MS, Thangam R, Sakthidhasan P, et al. (2018). Combined effect of a natural flavonoid rutin from Citrus sinensis and conventional antibiotic gentamicin on Pseudomonas aeruginosa biofilm formation. Food Control 90:282–94.

Du DJ, Wang-Kan X, Neuberger A, et al. (2018). Multidrug efflux pumps: structure, function and regulation. Nat Rev Microbiol 16:523–39.

Felicetti T, Cannalire R, Burali MS, et al. (2017). Searching for novel inhibitors of the *S. aureus* NorA efflux pump: synthesis and biological evaluation of the 3-phenyl-1,4-benzothiazine analogues. ChemMedChem 12:1293–302.

Felicetti T, Cannalire R, Pietrella D, et al. (2018). 2-Phenylquinoline S. aureus NorA efflux pump inhibitors: evaluation of the importance of methoxy group introduction. J Med Chem 61:7827–48.

Fernández L, Hancock RE. (2012). Adaptive and mutational resistance: role of porins and efflux pumps in drug resistance. Clin Microbiol Rev 25:661–81.

Foster TJ. (2017). Antibiotic resistance in *Staphylococcus aureus*. Current status and future prospects. FEMS Microbiol Rev 41:430–49.

Gao G, Jiang YW, Jia HR, et al. (2019). Near-infrared light-controllable on-demand antibiotics release using thermo-sensitive hydrogel-based drug reservoir for combating bacterial infection. Biomaterials 188:83–95.

Gold K, Slay B, Knackstedt M, et al. (2018). Antimicrobial activity of metal and metal-oxide based nanoparticles. Adv Therap 1:1700033.

Holler JG, Christensen SB, Slotved HC, et al. (2012). Novel inhibitory activity of the *Staphylococcus aureus* NorA efflux pump by a kaempferol rhamnoside isolated from Persea lingue Nees. J Antimicrob Chemoth 67:1138–44.

Kim JH, Yi YS, Kim MY, et al. (2017). Role of ginsenosides, the main active components of Panax ginseng, in inflammatory responses and diseases. J Ginseng Res 41:435–43.

Kumar S, Lekshmi M, Parvathi A, et al. (2020). Functional and structural roles of the major facilitator superfamily bacterial multidrug efflux pumps. Microorganisms 8:266.

LaBreck PT, Bochi-Layec AC, Stanbro J, et al. (2020). Systematic analysis of efflux pump-mediated antiseptic resistance in *Staphylococcus aureus* suggests a need for greater antiseptic stewardship. mSphere 5:e00959–e00919.

Lakhundi S, Zhang KY. (2018). Methicillin-resistant *Staphylococcus aureus*: molecular characterization, evolution, and epidemiology. Clin Microbiol Rev 31:e00018–00020.

Langeveld WT, Veldhuizen EJ, Burt SA. (2014). Synergy between essential oil components and antibiotics: a review. Crit Rev Microbiol 40:76–94.

Lee H, Lee S, Jeong D, et al. (2018). Ginsenoside Rh2 epigenetically regulates cell-mediated immune pathway to inhibit proliferation of MCF-7 breast cancer cells. J Ginseng Res 42:455–62.

Li YH, Su TT, Zhang Y, et al. (2015). Liposomal co-delivery of daptomycin and clarithromycin at an optimized ratio for treatment of methicillin-resistant *Staphylococcus aureus* infection. Drug Deliv 22:5.

Liu YF, Wang LJ, Liu JP, et al. (2013). A study of human skin and surface temperatures in stable and unstable thermal environments. J Therm Biol 38:440–8.

Lu C, Quan GL, Su M, et al. (2019). Molecular architecture and charging effects enhance the in vitro and in vivo performance of multi-arm antimicrobial agents based on star-shaped poly(L-Lysine). Adv Therap 2:1900147.

Matthew JE, Nazario YL, Roberts SC, et al. (2002). Effect of mammalian cell culture medium on the gelation properties of Pluronic® F127. Biomaterials 23:4615–9.

Mei LL, Chen JT, Yu SQ, et al. (2017). Expansible thermal gelling foam aerosol for vaginal drug delivery. Drug Deliv 24:1325–37.

Mir M, Ahmed N, Permana AD, et al. (2019). Enhancement in site-specific delivery of carvacrol against methicillin resistant *Staphylococcus aureus* induced skin infections using enzyme responsive nanoparticles: a proof of concept study. Pharmaceutics 11:606.

Mona GA, Hadeel AM, Nagia NA. (2020). Preparation of PLGA-chitosan based nanocarriers for enhancing antibacterial effect of ciprofloxacin in root canal infection. Drug Deliv 27:26–39.

Ng VW, Ke XY, Lee AL, et al. (2013). Synergistic co-delivery of membrane-disrupting polymers with commercial antibiotics against highly opportunistic bacteria. Adv Mater 25:6730–6.

Palazzotti D, Bissaro M, Bolcato G, et al. (2019). Deciphering the molecular recognition mechanism of multidrug resistance *Staphylococcus aureus* NorA efflux pump using a supervised molecular dynamics approach. IJMS 20:4041.

Pei YH, Mohamed MF, Seleem MN, et al. (2017). Particle engineering for intracellular delivery of vancomycin to methicillin-resistant *Staphylococcus aureus* (MRSA)-infected macrophages. J Control Release 267:133–43.

Redgrave LS, Sutton SB, Webber MA, et al. (2014). Fluoroquinolone resistance: mechanisms, impact on bacteria, and role in evolutionary success. Trends Microbiol 22:438–45.

Rowe SE, Wagner NJ, Li LP, et al. (2020). Reactive oxygen species induce antibiotic tolerance during systemic *Staphylococcus aureus* infection. Nat Microbiol 5:282–9.

Russo A, Concia E, Cristini F, et al. (2016). Current and future trends in antibiotic therapy of acute bacterial skin and skin-structure infections. Clin Microbiol Infect 22:S27–S36.

Schindler BD, Jacinto PL, Buensalido JA, et al. (2015). Clonal relatedness is a predictor of spontaneous multidrug efflux pump gene overexpression in *Staphylococcus aureus*. Int J Antimicrob Agents 45:464–70.

Sharma M, Sahu K, Singh SP, et al. (2018). Wound healing activity of curcumin conjugated to hyaluronic acid: in vitro and in vivo evaluation. Artif Cells Nanomed Biotechnol 46:1009–17.

Shriram V, Khare T, Bhagwat R, et al. (2018). Inhibiting bacterial drug efflux pumps via phyto-therapeutics to combat threatening antimicrobial resistance. Front Microbiol 9:2990

Singer AJ, Talan DA. (2014). Management of skin abscesses in the era of methicillin-resistant *Staphylococcus aureus*. N Engl J Med 370:1039–47.

Singh S, Kalia NP, Joshi P, et al. (2017). Boeravinone B, a novel dual inhibitor of NorA bacterial efflux pump of *Staphylococcus aureus* and human P-glycoprotein, reduces the biofilm formation and intracellular invasion of bacteria. Front Microbiol 8:1868

Tong SY, Davis JS, Eichenberger E, et al. (2015). *Staphylococcus aureus* infections: epidemiology, pathophysiology, clinical manifestations, and management. Clin Microbiol Rev 28:603–61.

Willers C, Wentzel JF, Du Plessis LH, et al. (2017). Efflux as a mechanism of antimicrobial drug resistance in clinical relevant microorganisms: the role of efflux inhibitors. Expert Opin Ther Targets 21:23–36.

Wright GD. (2017). Opportunities for natural products in 21st century antibiotic discovery. Nat Prod Rep 34:694–701.

Xu HJ, Huang SH, Wang JJ, et al. (2019). Enhanced cutaneous wound healing by functional injectable thermo-sensitive chitosan-based

hydrogel encapsulated human umbilical cord-mesenchymal stem cells. Int J Biol Macromol 137:433–41.

Xue P, Yang XS, Zhao L, et al. (2020). Relationship between antimicrobial activity and amphipathic structure of ginsenosides. Ind Crops Prod 143:111929.

Zeng YM, Chen JT, Li YR, et al. (2018). Thermo-sensitive gel in glaucoma therapy for enhanced bioavailability: in vitro characterization, in vivo pharmacokinetics and pharmacodynamics study. Life Sci 212:80–6.

Zhang JW, Sun Y, Wang YY, et al. (2014). Non-antibiotic agent ginsenoside 20(S)-Rh2 enhanced the antibacterial effects of ciprofloxacin in vitro and in vivo as a potential NorA inhibitor. Eur J Pharmacol 740:277–84.

Zhu CE, Huang Y, Zhang XY, et al. (2015). Comparative studies on exenatide-loaded poly (D,L-lactic-co-glycolic acid) microparticles prepared by a novel ultra-fine particle processing system and spray drying. Colloids Surf B 132:103–10.